Photometric Image-Based Rendering for Image Generation in Arbitrary Illumination

Yasuhiro MUKAIGAWA, Hajime MIYAKI, Sadahiko MIHASHI and Takeshi SHAKUNAGA
Department of Information Technology, Okayama University
Okayama-shi, Okayama 700-8530, JAPAN
{mukaigaw,shaku}@chino.it.okayama-u.ac.jp

Abstract

A Photometric Image-Based Rendering (PIBR) concept is proposed that facilitates the generation of an image with an arbitrary illumination. Based on this concept, we aim to generate both diffuse and specular reflections. It is not necessary to explicitly recover 3D shape and reflection properties of the scene. In order to control appearance changes caused by modifications in the lighting conditions, we utilize a set of real images taken in a variety of lighting conditions. Since the diffuse and specular reflection components have different characteristics, we separate these components and apply different methods to each. A photometric linearization is introduced to control diffuse reflections as well as for separating the other components. This also facilitates the treatment of attached shadows as a part of the diffuse reflection. A morphing technique is utilized to generate specular reflections. This is an effective technique for dealing with glossy objects, even when the light shape is clearly observed in the specular reflection. Experimental results show that realistic images can be successfully generated using this technique.

1. Introduction

The generation of images in arbitrary lighting conditions is one of the most important themes in Computer Graphics. For this purpose, Model-Based Rendering (MBR) is widely used[1], and it works well with a scene model consisting of 3D shapes, reflection properties and lighting conditions. However, an accurate model cannot be easily obtained without using special devices such as a high precision range finder.

To overcome some of the issues surrounding MBR, considerable work has been accomplished in the field of Image-Based Rendering (IBR). IBR is used to generate a new image from a set of real images without using accurate models. Since IBR makes full use of real images, a realistic image can be generated. However, almost all of the IBR approaches are classified as Geometric Image-Based Rendering (GIBR), which covers only geometric appearance changes caused by the change in view point. Although appearance changes caused by lighting condition changes are also important factors, many conventional IBR approaches cannot handle them. In order to control lighting conditions in the IBR framework, we propose a new concept called Photometric Image-Based Rendering (PIBR). An image, which should be taken in a particular lighting condition, is generated directly from a set of real images taken in a variety of lighting conditions. PIBR requires neither explicit 3D shape nor lighting models.

Lin-Lee[2][3] proposed some methods which generate specular reflections under arbitrary lighting conditions without explicit reconstruction of the surface normals and the surface reflectances. While these methods can avoid the reconstruction of parameters in the reflection model, they depend on the Torrance-Sparrow reflection model. Therefore, it is difficult to apply them to a glossy surface when a light shape is observed in the specular reflection.

In this paper, we propose a new PIBR method for generating not only diffuse reflections but also specular reflections of a glossy object. In this method, we use a set of real images taken by a fixed camera in a variety of lighting conditions. The aim of this technique is to generate realistic images in arbitrary lighting directions within the framework of IBR. A photometric linearization is introduced to control diffuse reflections and to separate the other components. A morphing technique is utilized to generate specular reflections.

2. Reflection models for PIBR

2.1. Classification of component

The major components of appearance changes due to lighting conditions are reflections and shadows. Ac-

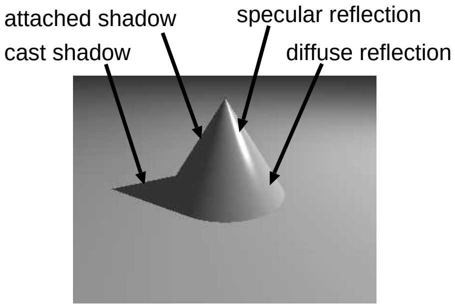

Figure 1. Major components of appearance changes.

cording to the dichromatic reflection model[4], reflections are classified into diffuse (body) reflections and specular (surface) reflections as shown in Fig.1. The two kinds of reflections have quite different characteristics. The diffuse reflection does not depend on viewing direction, and is observed equally from any direction. The specular reflection is observed intensely from the mirror direction of the incident direction.

Shadows are also classified into attached shadows and cast shadows[5]. Attached shadows depend on the angle between the surface normal and lighting direction, and are observed where the surface does not face the light source. Cast shadows depend on the whole 3D shape of the scene, and are observed where light is occluded by other objects.

2.2. Diffuse reflection model

The basic reflection model, comprising only diffuse reflections, is called the Lambertian reflection model. In the model, an intensity i on the surface is simply formulated by

$$i = \boldsymbol{n} \cdot \boldsymbol{s}. \tag{1}$$

In Eq.(1), $\boldsymbol{n}$ denotes the surface property vector which is a product of a unit normal vector and a diffuse reflectance, and $\boldsymbol{s}$ denotes the lighting property vector which is a product of a unit vector along the lighting direction and the lighting power.

In Eq.(1), if the angle between $\boldsymbol{n}$ and $\boldsymbol{s}$ is greater than 90°, the intensity i becomes negative. In this case, the attached shadow appears on the object and the intensity should be zero instead of the negative value. In order to deal with attached shadows as well as diffuse reflections, Eq.(2) is used instead[6].

$$i = max(\boldsymbol{n} \cdot \boldsymbol{s}, 0) \tag{2}$$

In this reflection model, the intensity does not change significantly when $\boldsymbol{n}$ and $\boldsymbol{s}$ slightly changes. Therefore, this model is stable against errors included in the lighting direction and surface normals.

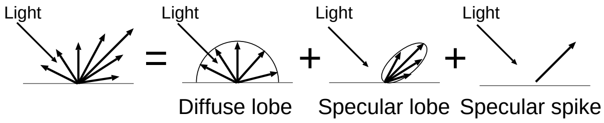

Figure 2. Reflection models.

2.3. Specular reflection model

Specular reflections are modeled as a combination of specular lobes and specular spikes as shown in Fig.2. Specular spikes are usually ignored because they are only observed from very narrow angles. Specular lobe is modeled in both the Torrance-Sparrow and Phong models. Since the intensity of a pixel is subject to significant changes even if model parameters change only slightly, parameter estimation tends to be unstable. Moreover, it is difficult to express a light shape observed on a glossy surface using these simple models.

2.4. Component classification in PIBR

In this paper, we deal with both diffuse and specular reflections. As mentioned above, we regard attached shadows as a part of diffuse reflections. Although we cannot generate cast shadows because they require the entire 3D model of the scene, we can use input images that include cast shadows.

In the IBR framework, we aim to generate diffuse and specular reflections in arbitrary lighting conditions. We assume that input images are taken in a variety of lighting conditions by a fixed camera, and the lighting directions are unknown. Since the diffuse reflections and the specular reflections have different characteristics, we separate these components and apply a different technique to each component.

For diffuse reflections, we basically use the Lambertian reflection model. The surface normal, however, cannot be determined uniquely because we assume that the lighting directions are unknown. Therefore, we introduce a photometric linearization method to generate diffuse reflections without using explicit surface normals and lighting directions.

For specular reflections, we do not use any general reflection models. If the object is very glossy, a light shape is observed in the specular reflection. This phenomenon cannot be reproduced by simple reflection models. Therefore, we utilize a morphing technique to generate the specular reflections.

3. Diffuse reflection in PIBR

3.1. Linear combination

If the Lambertian reflection model is assumed, a simple algorithm works well for image generation. If both the target objects and the viewing position are fixed, the observed image depends only on the lighting direction. Shashua[5] shows that if a single point light source is assumed at infinity, the image $\boldsymbol{I}_k$ can be generated with any lighting directions using a linear combination of three base images ($\boldsymbol{I}_1$, $\boldsymbol{I}_2$, $\boldsymbol{I}_3$) taken in different lighting directions,

$$\boldsymbol{I}_k = c_k^1 \boldsymbol{I}_1 + c_k^2 \boldsymbol{I}_2 + c_k^3 \boldsymbol{I}_3. \tag{3}$$

Here, let $\boldsymbol{c}_k = [c_k^1 \ c_k^2 \ c_k^3]^T$ be a set of coefficients of the image $\boldsymbol{I}_k$.

The diffuse component under any lighting direction can be easily generated by a linear combination of three base images without using any 3D shape models. However, this approach assumes that the image contains no specular reflections or shadows. Therefore, it is difficult to apply the linear combination method to real scenes.

3.2. Photometric linearization

The real image often does not satisfy Eq.(1) due to specular reflections and shadows. Georghiades et al.[7] proposed a method for reconstructing surface normals of the real scene. In this method, both specular reflections and shadows are detected by thresholding, and surface normals and lighting directions are estimated by iteration of a singular value decomposition. The 3D shape of the target object is reconstructed from the surface normals, and the cast shadow regions are determined using a ray tracing technique.

On the other hand, we convert input images to imaginary images that satisfy Eq.(1). The converted images contain only diffuse components, and the pixels in the attached shadows have negative values that satisfy Eq.(1). Since the converted images satisfy Eq.(3), we call this conversion a photometric linearization. Basically, the photometric linearization in our method is similar to the estimation of surface normals proposed in [7]. Our approach, however, has an advantage that 3D shape models of the scene are unnecessary because specular components and cast shadows can be separated by Eq.(3).

Photometric linearization is realized by the following steps. First, three base images are selected from input images, and the coefficients of the linear combination are calculated for every input image. Next, the base images are linearized. Finally, all the input images are linearized, and specular components and cast shadows separated. The detailed algorithms are described in the following three sections.

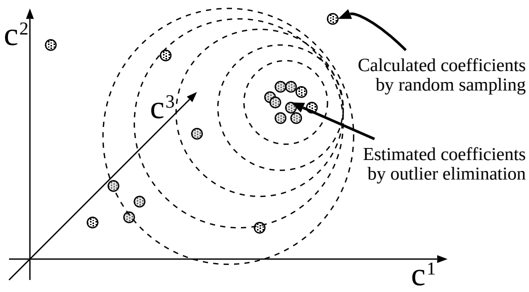

Figure 3. Estimation of the coefficients by random sampling and outlier elimination.

3.2.1 Coefficients of linear combination

Let $\boldsymbol{I}_1, \boldsymbol{I}_2, \cdots, \boldsymbol{I}_j$ denote the input images. First, three base images ($\boldsymbol{I}_1$, $\boldsymbol{I}_2$, $\boldsymbol{I}_3$), whose lighting directions are linearly independent, are selected from the input images. A set of coefficients, $\boldsymbol{c}_k$, for each input image $\boldsymbol{I}_k$ ($k = 4, \ldots, j$) can be calculated by selecting arbitrary three pixels from the images. If all the images include only diffuse components, unique coefficients are determined. Real scenes, however, include other components such as specular reflections and shadows. Therefore, Eq.(3) is not always satisfied.

In order to reliably calculate the coefficients of real images, we introduce an iterative method of random sampling and outlier elimination. Three pixels are randomly selected from the images, and the coefficients calculated. After iteration of this process, a coefficient distribution is obtained. If all the selected pixels include only diffuse components, the calculated coefficients center around the correct point in the coefficient space in a dense formation as shown in Fig.3. On the other hand, if the pixels include specular reflections or shadows, the coefficients are isolated from the correct point. Hence, the most reliable coefficients can be found by iterative calculation of a center of gravity and outlier elimination. The coefficients of the linear combination can be reliably estimated even if the input images contain specular reflections and shadows.

3.2.2 Photometric linearization of base images

Next, we linearize the base images using the estimated coefficients for each input image. Three images ($\boldsymbol{I}_l$, $\boldsymbol{I}_m$, $\boldsymbol{I}_n$), excluding the three base images, are selected from the input images. Since the coefficients ($\boldsymbol{c}_l$, $\boldsymbol{c}_m$,

$\boldsymbol{c}_n$) of the selected images have already been calculated, the base images ($\boldsymbol{I}_1$, $\boldsymbol{I}_2$, $\boldsymbol{I}_3$) can be regenerated by a linear combination of the selected input images and their coefficients. Let $\boldsymbol{I}_1^{(l,m,n)}$, $\boldsymbol{I}_2^{(l,m,n)}$ and $\boldsymbol{I}_3^{(l,m,n)}$ be the regenerated base images.

If a pixel contains only a diffuse component in all the selected images, the pixel in the regenerated image also contains only a diffuse component. Although real images include other components, they are observed within a limited lighting direction for each pixel. Hence, we use an iterative method again as follows: The candidates for pixel intensity of the linearized base images are calculated by a linear combination of three input images which are selected at random. After iteration of random selection and calculation, a pixel intensity distribution is obtained. The most reliable intensities are estimated in the same manner described in section 3.2.1. As a result, the three base images $\boldsymbol{I}_1$, $\boldsymbol{I}_2$ and $\boldsymbol{I}_3$ are linearized to $\boldsymbol{I}_1^L$, $\boldsymbol{I}_2^L$ and $\boldsymbol{I}_3^L$, respectively.

3.2.3 Separation of the other components

We have already obtained linearized base images ($\boldsymbol{I}_1^L$, $\boldsymbol{I}_2^L$, $\boldsymbol{I}_3^L$) and coefficients $\boldsymbol{c}_k$ for each input image $\boldsymbol{I}_k$. All input images can be easily linearized to $\boldsymbol{I}_4^L, \cdots, \boldsymbol{I}_j^L$ by linear combinations of the linearized base images with the coefficients. The specular components can then be separated by comparing each input image $\boldsymbol{I}_k$ with the linearized image $\boldsymbol{I}_k^L$. Assuming that there is no interreflection in the scene, specular regions can be distinguished by finding pixels whose intensities are brighter than the linearized image. In this method, specular components can be separated even if the color of the light source and the object surface is similar[5]. In the similar way, cast shadows can also be separated by finding pixels whose intensities are darker than the linearized image and are close to zero.

Although this approach assumes a single point light source at infinity, the Lambertian reflection model is stable against slight changes in the lighting direction as described in section 2.2. Therefore, stable linearization can be accomplished if the light source is far enough from the object.

3.3. Generation of diffuse components

Diffuse components can be easily generated by a linear combination of the linearized base images ($\boldsymbol{I}_1^L$, $\boldsymbol{I}_2^L$, $\boldsymbol{I}_3^L$). The generated image includes negative values in attached shadow regions. By replacing the negative values with zeros, we can generate attached shadows as well as diffuse components.

In order to generate arbitrarily illuminated images by a linear combination, different methods have been proposed based on principal component analysis (PCA)[8]. The PCA-based methods, however, do not provide any geometric relationship between lighting direction and the coefficients for orthogonal bases. All combinations of the geometric relationship should be stored for each input images in advance. Hence, it is difficult to directly control lighting direction using coefficients in the PCA-based methods. Some combinations of coefficients may generate impossible images. On the other hand, our method can analyze a geometric relationship between lighting direction and coefficients, therefore it is easy to specify lighting direction.

In our method, it was assumed that the lighting property vectors ($\boldsymbol{s}_1$, $\boldsymbol{s}_2$, $\boldsymbol{s}_3$) of the base images are unknown. Here, we introduce a 3×3 matrix $\boldsymbol{M}$, which transforms the lighting property vectors into the coefficients.

$$\begin{bmatrix} \boldsymbol{c}_1 & \boldsymbol{c}_2 & \boldsymbol{c}_3 \end{bmatrix} = \boldsymbol{M} \begin{bmatrix} \boldsymbol{s}_1 & \boldsymbol{s}_2 & \boldsymbol{s}_3 \end{bmatrix} \tag{4}$$

Since the actual lighting property vectors are unknown, the matrix $\boldsymbol{M}$ is also unknown[9]. The matrix $\boldsymbol{M}$ linearly transforms the orthonormal space in which the lighting property vector exists into a non-orthonormal space whose axes correspond to $\boldsymbol{c}_1$, $\boldsymbol{c}_2$ and $\boldsymbol{c}_3$. A linear relationship is satisfied between the actual lighting property vector $\boldsymbol{s}_k$ and the coefficients $\boldsymbol{c}_k$ of the linear combination as shown in

$$\boldsymbol{C} = \boldsymbol{M}\boldsymbol{S}, \tag{5}$$

where

$$\boldsymbol{C} = \begin{bmatrix} \boldsymbol{c}_1 & \boldsymbol{c}_2 & \cdots & \boldsymbol{c}_j \end{bmatrix}, \tag{6}$$

$$\boldsymbol{S} = \begin{bmatrix} \boldsymbol{s}_1 & \boldsymbol{s}_2 & \cdots & \boldsymbol{s}_j \end{bmatrix}. \tag{7}$$

Consequently, we can regard $\boldsymbol{c}_k$ as a lighting direction in the linearly transformed space. Although $\boldsymbol{S}$ and $\boldsymbol{M}$ are unknown, their product $\boldsymbol{C}$ is known. Hence, we can directly control the lighting direction by the relative direction of the input images instead of by interpolation. Moreover, if we specify arbitrary coefficients, impossible images are never generated, because the lighting property vector always exists for the coefficients.

Of course, if three lighting property vectors are accurately measured when the base images are captured, $\boldsymbol{M}$ can be calculated. Using the matrix, the given lighting property vector $\boldsymbol{s}_k$ is transformed into the coefficients $\boldsymbol{c}_k$. Thus, we can directly specify the lighting direction in the real space.

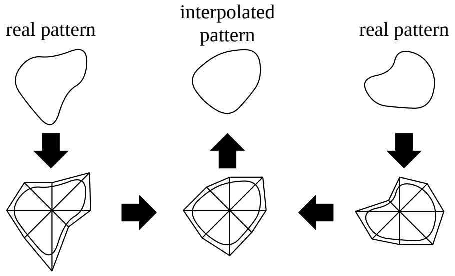

Figure 4. Morphing of specular regions.

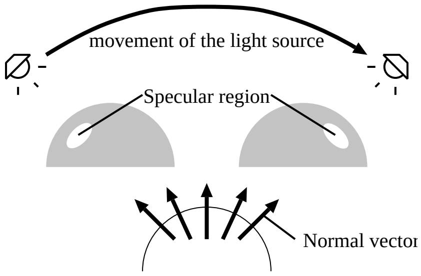

Figure 5. Transition of specular region.

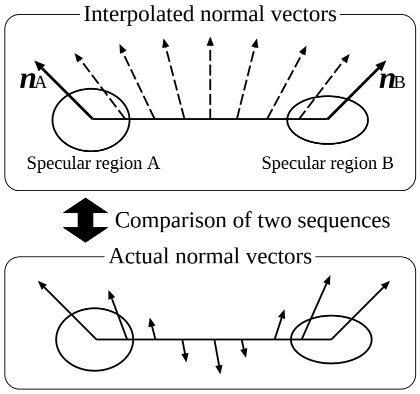

Figure 6. Corresponding specular regions.

4. Specular reflection in PIBR

4.1. Morphing of specular reflection

In order to generate specular reflection components in the framework of PIBR, we utilize a morphing technique. The separated specular components are approximated by polygons, and the corresponding specular regions are found in the input images. Then, both intensity and shape are linearly interpolated for every polygon as shown in Fig.4. The morphing technique has some advantages as follows:

(1) Morphing is based on only the correspondence of specular regions between input images. Therefore, we do not need lighting directions of the input images. This advantage is very significant.
(2) Morphing is available for glossy objects. The light shape is often observed as a specular reflection on very glossy surfaces. This complex phenomenon cannot be reproduced by simple reflection models. The morphing facilitates reproduction because real images are mapped as a texture.
(3) The intensity and the shape of the polygons are linearly interpolated. Therefore, the specular reflections change in a smooth motion when the light source moves.
(4) There is no guarantee that an accurate specular pattern is generated by interpolation. It is, however, easy to improve the accuracy of the generated image by increasing variegation in the input images.

4.2. Corresponding specular regions

In order to apply this morphing technique, it is necessary to find corresponding specular regions among input images. There is, however, no clear cue for the correspondence because specular reflection appears independently on each pixel. Hence, we have to define the pseudo correspondence of specular regions.

When a light source moves, the specular pattern gradually moves on the object surface, if the surface normal changes smoothly as shown in Fig.5. Here, we regard two specular regions in different images as corresponding to each other if the surface normal changes smoothly between the two regions.

In order to decide if two specular regions A and B correspond, we utilize the difference of two sequences of normal vectors as shown in Fig.6. One of the two sequences is generated by linear interpolation of two normal vectors $\boldsymbol{n}_A$ and $\boldsymbol{n}_B$ at the center of gravity of regions A and B. The other is the actual surface normal observed between the two regions. We regard the two regions as corresponding to each other only if the difference of sequences is the minimum in the set of all possible combinations and is smaller than a threshold.

Using the difference of sequences, we can find corresponding specular regions. The surface normals, however, cannot be uniquely reconstructed because we assume that the lighting directions of the input images are unknown. Therefore, some clues are necessary to estimate the smoothness of surface normals.

Here, let $\boldsymbol{n}_1 \cdots \boldsymbol{n}_t$ denote the actual surface property vectors of all the pixels, where t is the number of pixels included in the images, and the actual value of $\boldsymbol{n}_i$ is unknown. By Eq.(5), an image matrix $\boldsymbol{I}$ can be expressed as follows:

$$\begin{aligned} \boldsymbol{I} &= \boldsymbol{N}\boldsymbol{S} & (8)\\ &= (\boldsymbol{N}\boldsymbol{M}^{-1})(\boldsymbol{M}\boldsymbol{S}) & (9)\\ &= (\boldsymbol{N}\boldsymbol{M}^{-1})\boldsymbol{C}. & (10) \end{aligned}$$

Here,

$$\boldsymbol{I} = \begin{bmatrix} \boldsymbol{I}_1^L & \boldsymbol{I}_2^L & \cdots & \boldsymbol{I}_j^L \end{bmatrix}, \tag{11}$$

$$\boldsymbol{N} = \begin{bmatrix} \boldsymbol{n}_1 & \boldsymbol{n}_2 & \cdots & \boldsymbol{n}_t \end{bmatrix}^T. \tag{12}$$

Consequently, Eq.(8) indicates that input images are expressed as a product of the surface property vectors and the lighting property vectors. On the other hand, Eq.(10) suggests that the images are also expressed as a product of the coefficients and the surface property vectors which are transformed by the matrix $\boldsymbol{M}^{-1}$. Here, $\boldsymbol{c}_1 = [1\ 0\ 0]^T$, $\boldsymbol{c}_2 = [0\ 1\ 0]^T$ and $\boldsymbol{c}_3 = [0\ 0\ 1]^T$ according to Eq.(3). These coefficients and Eq.(10) lead to

$$\boldsymbol{N}\boldsymbol{M}^{-1} = [\boldsymbol{I}_1^L\ \boldsymbol{I}_2^L\ \boldsymbol{I}_3^L]. \tag{13}$$

This equation indicates that the surface property vectors transformed by the matrix $\boldsymbol{M}^{-1}$ are equal to the matrix that consists of the three linearized base images. Although both $\boldsymbol{N}$ and $\boldsymbol{M}^{-1}$ are unknown, we can calculate the product of the two matrices because we can obtain $\boldsymbol{I}_1^L$, $\boldsymbol{I}_2^L$, $\boldsymbol{I}_3^L$ by using photometric linearization.

Although the surface property vectors cannot be uniquely reconstructed if the lighting directions are unknown[6][7][9], continuity of the normals is maintained even if the vectors are transformed linearly. Therefore, we can utilize the continuity of the intensities in the linearized base images for finding corresponding regions instead of surface property vectors.

5. Experimental results

This section presents the results of image generation tests using a glossy ceramic pot under a single light source. Keeping a halogen light away from the pot, twenty four images were captured with changing lighting directions in a darkroom.

First, three base images were selected from the input images as shown in the left column of Fig.7, and the coefficients set to [1 0 0], [0 1 0] and [0 0 1], respectively. The input images include specular reflections as well as shadows. The right column of Fig.7 shows the results of photometric linearization of the base images. Since the linearized images have negative values, a zero level

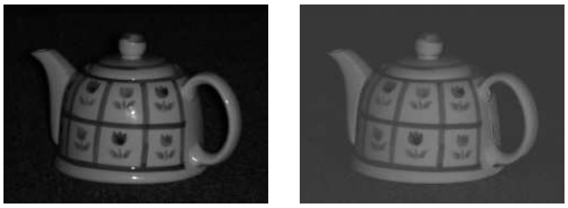

(a) [1 0 0]

(b) [0 1 0]

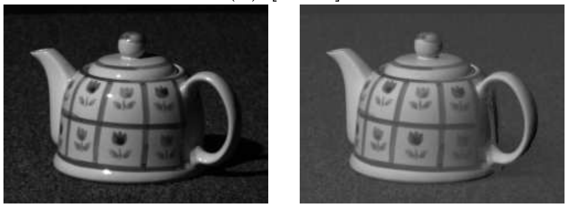

(c) [0 0 1]

Figure 7. Three base images (Left: input images, Right: linearized base images).

is expressed as a gray intensity in these images. In the linearized images, specular reflections and cast shadows are correctly eliminated, and the pixel value is negative in attached shadows. Some discontinuities were found in the images because the pixels were not illuminated in every input image.

Next, all input images were linearized using the linearized base images. Figures 8(a) and (b) show examples of the input images and the results of photometric linearization, respectively. It can be seen that the input images are linearized with the exception of some regions for which the base images were not correctly linearized. Figure 8(c) and (d) show the separated specular regions. Although the separated regions include some noise, large regions are correctly approximated by polygons.

Using the proposed method, we generated a new image whose lighting direction was not included in the input image set. As shown in Table 1, coefficients were specified by interpolation of the neighboring two input images. The intermediate coefficients were linearly interpolated, and the lighting power normalized. The left column of Fig.9 shows the generated images with diffuse reflections by linear combination. Specular reflections were generated by morphing, as shown in the right column of Fig.9. Appropriate surface properties

Table 1. Coefficients of linear combination.

	(a)			(b)			(c)		
Two input images	[0.569	–0.313	0.991]	[0.562	1.063	–0.265]	[–0.510	0.298	0.910]
	[–0.095	–0.407	1.094]	[0.268	0.875	0.332]	[–0.320	0.509	0.674]
Synthesized images	[0.248	–0.376	1.088]	[0.434	1.013	0.035]	[–0.420	0.409	0.803]

(a) Examples of input images

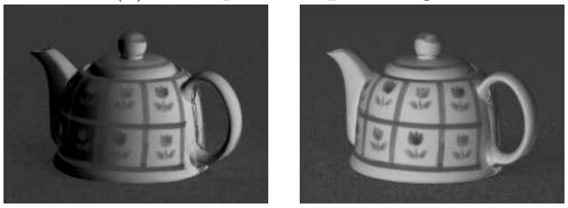

(b) Linearized images

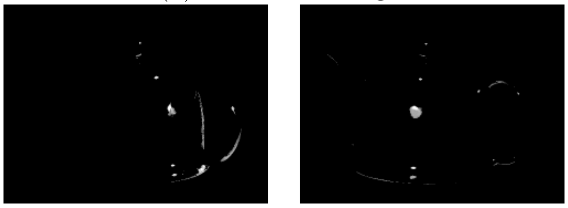

(c) Separated specular components

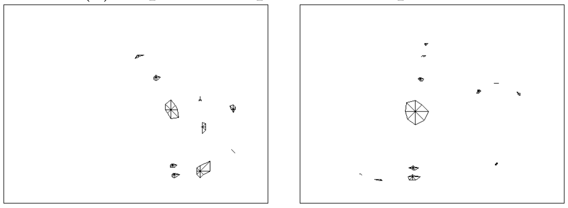

(d) Specular regions approximated by polygons

Figure 8. Linearization of the input images and separation of specular components.

(a) [0.248 –0.376 1.088]

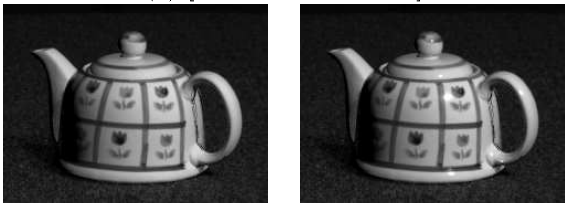

(b) [0.434 1.013 0.035]

(c) [–0.420 0.409 0.803]

Figure 9. Generated images (Left: only diffuse reflections, Right: diffuse and specular reflections).

are observed in the generated images.

In order to illustrate the effectiveness of morphing, we compared it with a standard PCA-based method. As shown in Fig.10, a sequence of specular components were generated with changing lighting directions. The PCA-based method generates unnatural patterns because the location of the specular pattern is fixed during light movement resulting in a simple interpolation of intensity. On the other hand, the new morphing-based method can generate natural patterns from a small number of input images because both intensity and location can be changed smoothly.

Finally, experimental results are presented for a scene where linear light shapes are observed in the specular reflection. As shown in Fig.11(a), twenty eight images of a glossy ceramic pot were captured while changing the position of a fluorescent lamp. Figure 11(b) and (c) show the results of photometric linearization and the results of separation of the specular components respectively. Separations are successfully accomplished, even if light shapes were observed. The generated images with both diffuse and specular reflections are shown in Fig.11(d). Generally, it is difficult to reliably estimate parameters of the reflection models if the illumination is not a point light source. Our method, however, makes full use of real images in the morphing process. Therefore, the light shapes can be reproduced with greater accuracy.

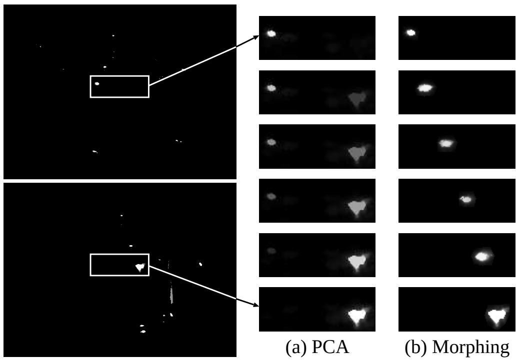

Figure 10. Transition of specular patterns.

6. Conclusions

In this paper, we proposed a concept of Photometric Image-Based Rendering which facilitates the generation of images in arbitrary lighting conditions from a set of real images. We provided a strategy to generate both diffuse and specular reflections within the framework of PIBR. We introduced a photometric linearization for the generation of diffuse reflections with attached shadows, and utilized a morphing technique for the generation of specular reflections.

From experimental results using real images, we confirmed that PIBR is a suitable technique with scenes that include specular reflections. We also confirmed that morphing is effective for images containing glossy objects where the light shape is observed in specular reflections. This ability is important because it cannot always be assumed that the point light source is at infinity. Since PIBR can generate realistic images that are almost indistinguishable from real images, it is can be used for many applications.

In the future, we will attempt to generate interreflections and cast shadows within the PIBR framework. We will also try to model not only lighting condition changes but also view position changes by a combination of PIBR and GIBR.

Acknowledgment

A part of this research has been supported by Japan Science and Technology Corporation under Ikeuchi CREST project.

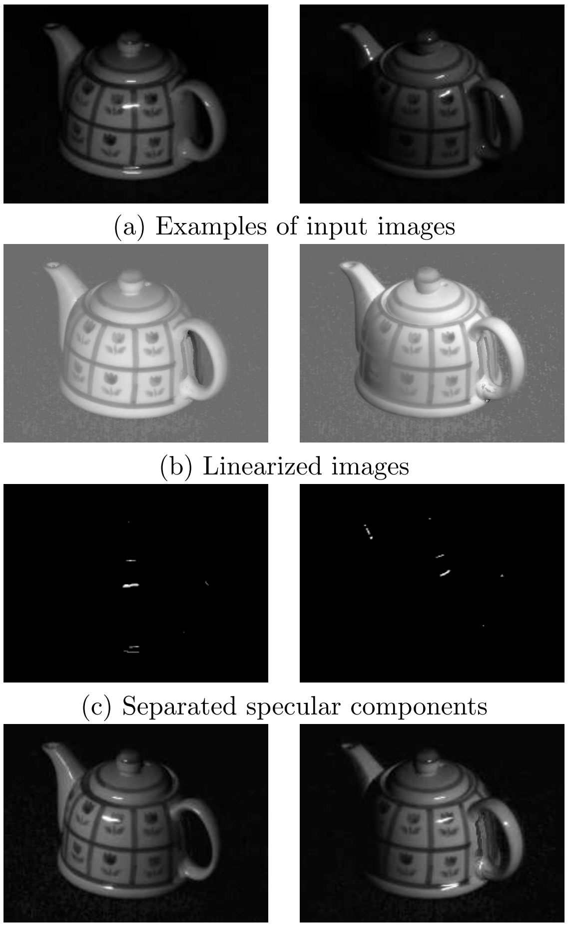

(a) Examples of input images

(b) Linearized images

(c) Separated specular components

(d) Generated images

Figure 11. Image generation in the complex scene.

References

[1] Y.Sato, M.Wheeler and K.Ikeuchi: Object Shape and Reflectance Modeling from Observation, Proc. SIGGRAPH'97, pp.379-387 (1997).

[2] S.Lin and S.W.Lee: A Representation of Specular Appearance, Proc. IEEE International Conference on Computer Vision (ICCV'99), pp.849-854 (1999).

[3] S.Lin and S.W.Lee: Estimation of Diffuse and Specular Appearance, Proc. IEEE International Conference on Computer Vision (ICCV'99), pp.855-860 (1999).

[4] S.A.Shafer: Using color to separate reflection components, Color Research and Application, Vol.10, pp.210-218 (1985).

[5] A.Shashua: Geometry and Photometry in 3D Visual Recognition, Ph.D thesis, Dept. Brain and Cognitive Science, MIT (1992).

[6] P.N.Belhumeur and D.J.Kriegman: What is the Set of Images of an Object Under All Possible Lighting Conditions?, Proc. IEEE Conference on Computer Vision and Pattern Recognition (CVPR'96), pp.270-277 (1996).

[7] A.S.Georghiades, D.J.Kriegman and P.N.Belhumeur: Illumination Cones for Recognition Under Variable Lighting: Faces, Proc. IEEE Conference on Computer Vision and Pattern Recognition (CVPR'98), pp.52-58 (1998).

[8] Z.Zhang: Modeling Geometric Structure and Illumination Variation of a Scene from Real Images, Proc. IEEE International Conference on Computer Vision (ICCV'98), pp.1041-1046 (1998).

[9] P.N.Belhumeur, D.J.Kriegman and A.L.Yuille: The Bas-Relief Ambiguity, International Journal of Computer Vision, 35(1), pp.33-44 (1999).